

See discussions, stats, and author profiles for this publication at: <https://www.researchgate.net/publication/260105037>

# Acetic Acid Adsorption on Anatase TiO<sub>2</sub> (101)

ARTICLE *in* THE JOURNAL OF PHYSICAL CHEMISTRY C · MAY 2012

Impact Factor: 4.77 · DOI: 10.1021/jp303514g

---

CITATIONS

17

---

READS

45

## 3 AUTHORS, INCLUDING:



David Grinter

Brookhaven National Laboratory

15 PUBLICATIONS 100 CITATIONS

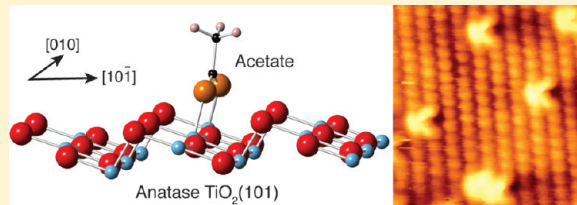
SEE PROFILE

# Acetic Acid Adsorption on Anatase $\text{TiO}_2(101)$

David C. Grinter, Marco Nicotra, and Geoff Thornton\*

London Centre for Nanotechnology and Chemistry Department, University College London, London WC1H 0AH, United Kingdom

**ABSTRACT:** The adsorption and reactivity of acetic acid on anatase  $\text{TiO}_2(101)$  has been investigated with scanning tunneling microscopy (STM). At low coverage, acetic acid is observed to have a characteristic appearance in STM consistent with a dissociative bidentate binding geometry. At room temperature acetic acid has a relatively strong interaction with the anatase (101) surface and a near-unity sticking probability. When deposited at elevated temperatures (420 K), a saturated coverage displays a partially ordered superstructure with two domains across small regions of the anatase surface. The periodicity of these domains was found to be  $(2 \times 1)$ , again consistent with a bidentate binding geometry of the acetate to two neighboring  $\text{Ti}_{\text{sc}}$  sites along the [010] direction. Heating the acetate-covered surface to 570 K in ultrahigh vacuum resulted in clean desorption of ~90% of the molecules, leaving only a small fraction undesorbed that were mainly situated at the step edges of the anatase. STM tip pulsing of +6 V was also found to desorb acetate molecules from the surface.



## INTRODUCTION

Applications of  $\text{TiO}_2$  are numerous and well-documented, with important examples including heterogeneous catalysis, dye-sensitized solar cells, pigments, optical coatings, gas sensing, and even gate materials in semiconducting devices such as memristors.<sup>1–6</sup> The photocatalytic behavior of  $\text{TiO}_2$  in particular, first discovered by Fujishima and Honda,<sup>7</sup> has driven research into the various surfaces of titania. In particular, rutile  $\text{TiO}_2(110)(1 \times 1)$  has become the prototypical metal oxide termination for studies of surface reconstructions, defects, adsorbates, and many other phenomena. In spite of the wealth of work in the literature on rutile  $\text{TiO}_2$ , arguably the most active polymorph for catalysis and that which is found in most nanomaterials employed in commercial applications is actually the anatase form.<sup>4</sup> Reasons for the relative paucity of detailed experimental work on the surfaces of anatase  $\text{TiO}_2$  include difficulty in preparing good-quality, large, artificial crystals and the poor availability of large natural mineral crystals with suitably low levels of contaminants. As a result of these problems, one alternative approach has been to grow thin films of anatase  $\text{TiO}_2$  via molecular beam epitaxy (MBE) or chemical vapor deposition (CVD) on suitable substrates, examples of which include  $\text{SrTiO}_3(100)$  and  $\text{LaAlO}_3(100)$ .<sup>8,9</sup>

Anatase and rutile  $\text{TiO}_2$  display quite different chemistry at their surfaces, an example of which is their behavior toward water. This is found to adsorb molecularly on anatase  $\text{TiO}_2(101)$  but dissociatively at low coverages on rutile  $\text{TiO}_2(110)$ .<sup>10,11</sup> The (101) surface of anatase  $\text{TiO}_2$  is the thermodynamically most stable and makes up the major fraction of industrial catalysts.<sup>4</sup> Its basic structure and the interaction with water and precious metal deposition have been studied previously using scanning tunneling microscopy (STM) and low-energy electron diffraction (LEED).<sup>10,12,13</sup> An interesting point to note is the relatively low density of point defects such as surface oxygen vacancies observed on anatase  $\text{TiO}_2(101)$  in comparison with rutile

$\text{TiO}_2(110)$ , as well as the relative importance of step edges in the reactivity of anatase.<sup>14</sup> Step edges and other defect sites are very important features generally in the study of oxide surfaces. They are involved in a number of processes such as adsorption of molecules, nucleation sites for metal particles, and crystal growth. The adsorption of small molecules on the surfaces of metal oxides, and  $\text{TiO}_2$  in particular, is of great interest from the standpoint of investigating both their catalytic behavior and their fundamental adsorption properties. One important class of molecules for these studies is carboxylic acids, whose functionality and strong bonding to oxide surfaces play a role in linking dye molecules to  $\text{TiO}_2$  for use in solar cells and the formation of self-assembled monolayers and as organic linkers in large organic–inorganic frameworks.<sup>15–20</sup> The behavior of carboxylic acids is well documented on rutile  $\text{TiO}_2$  surfaces,<sup>3</sup> but there is a lack of experimental data for their adsorption on anatase bar some studies on polycrystalline samples.<sup>21,22</sup>

In this work a natural mineral anatase  $\text{TiO}_2(101)$  crystal was used which was translucent and had a dark blue color similar to that of a heavily reduced rutile  $\text{TiO}_2(110)$  single crystal. A slight contamination of unknown origin manifested itself as an orange tint in some parts of the crystal, although it did not appear to affect our studies and was below the detection level of Auger electron spectroscopy (AES) of the surface region. In this work we provide an examination of both low and high acetic acid coverage of the anatase  $\text{TiO}_2(101)$  surface and suggest a model for the binding.

## EXPERIMENTAL PROCEDURE

The STM, LEED, and AES experiments were all conducted in an ultra-high-vacuum (UHV) chamber with a base pressure of  $1 \times$

Received: April 12, 2012

Revised: May 11, 2012

Published: May 12, 2012



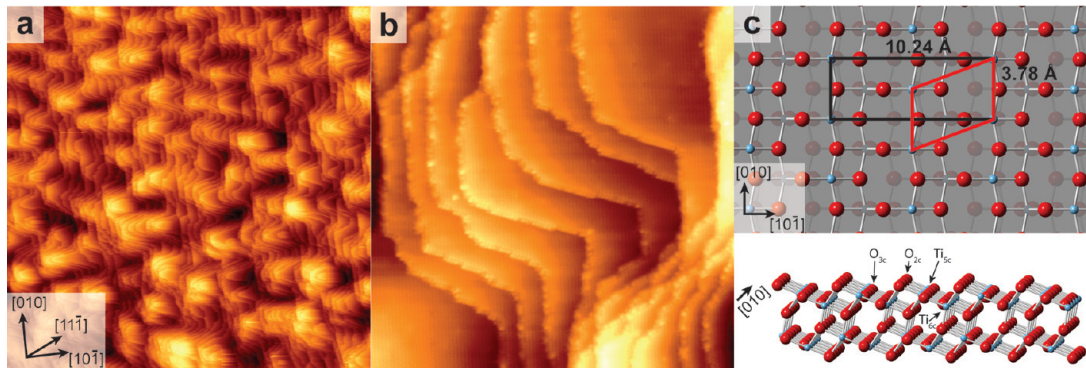


**Figure 1.** STM images and models of the clean anatase  $\text{TiO}_2(101)$  surface. (a) Large-area image ( $300 \times 300 \text{ nm}^2$ ,  $V_s = +1.2 \text{ V}$ ,  $I_t = 0.40 \text{ nA}$ ) obtained after cycles of sputtering and annealing displaying typical (101) terraces with step edges oriented parallel to  $[010]$ ,  $[1\bar{1}\bar{1}]$ , and  $[1\bar{1}\bar{1}]$ . (b) Small-area image ( $50 \times 50 \text{ nm}^2$ ,  $V_s = +1.2 \text{ V}$ ,  $I_t = 0.20 \text{ nA}$ ) showing the monatomic steps with faint contrast of the atomic lattice. (c) Ball-and-stick models of the anatase  $\text{TiO}_2(101)$  surface in both plan (top) and side (bottom) views. Key: red, oxygen; blue, titanium. The centered rectangular and primitive surface unit cells are marked in black and red, respectively, and the “sawtooth” structure of the surface is clearly visible in the lower model.

$10^{-11}$  mbar attached to a separate sample preparation chamber equipped for  $\text{Ar}^+$  sputtering, electron bombardment heating, residual gas analysis (RGA) mass spectrometry, and gas and metal dosing. The STM instrument employed was an Omicron UHV atomic force microscope/scanning tunneling microscope operated in constant-current mode at room temperature using electrochemically etched tungsten tips that were conditioned during scanning with voltage pulses up to 10 V and high bias scans. The natural mineral anatase  $\text{TiO}_2(101)$  crystal (Pi-Kem) was attached to a standard sample plate with spot-welded tantalum clips and the temperature during annealing monitored using an infrared pyrometer (Land). Temperatures lower than the minimum limit of the pyrometer ( $\sim 750 \text{ K}$ ) were measured by a K-type thermocouple attached to the manipulator arm and positioned near the sample plate. Cycles of  $\text{Ar}^+$  sputtering (20 min, 1 keV, 10  $\mu\text{A}$ ) and UHV annealing (5–20 min, 880–1000 K) were employed to clean the sample until any contamination was below the detection limit of AES and a well-ordered anatase  $\text{TiO}_2(101)(1 \times 1)$  LEED pattern with a low background was observed, yielding a surface suitable for atomic resolution STM imaging. The STM data were calibrated by comparison with atomically resolved images of the rutile  $\text{TiO}_2(110)(1 \times 1)$  surface obtained just prior to these experiments.

Acetic acid (99.99%, Sigma-Aldrich) was contained within a glass vial attached to the gas line of the UHV system and admitted into the preparation chamber via a high-precision leak valve. Several freeze–pump–thaw cycles were carried out to purify the acetic acid. All exposures are nominal and quoted in langmuirs (1 langmuir =  $1.33 \times 10^{-6} \text{ mbar s}$ ) on the basis of the uncompensated pressure within the preparation chamber during dosing. In this work, a monolayer (ML) is defined by the number of  $\text{Ti}_{5c}$ – $\text{O}_{2c}$  pairs on the ideal (101) surface, which corresponds to a density of  $5.17 \text{ nm}^{-2}$ . For exposures in the range 0.05–0.5 langmuir an uncompensated chamber pressure of  $1.0 \times 10^{-9} \text{ mbar}$  was used. For the range of 1.0–15 langmuirs the chamber pressure was  $5 \times 10^{-8} \text{ mbar}$ .

## RESULTS AND DISCUSSION

**Clean Anatase  $\text{TiO}_2(101)$ .** Cycles of sputtering and annealing in UHV led to a well-ordered ( $1 \times 1$ ) LEED pattern with spacings consistent with previous results for anatase  $\text{TiO}_2(101)$ .<sup>14,23</sup> STM images of the anatase  $\text{TiO}_2(101)$  surface after a number of annealing cycles are displayed in Figure 1a,b, where it is observed that the sample displays a heavily stepped

structure with (101) terraces up to 30 nm wide separated by monatomic steps of height 0.38 nm. The step edges are primarily oriented parallel to the  $[1\bar{1}\bar{1}]$  and  $[1\bar{1}\bar{1}]$  directions with some shorter edges oriented parallel to  $[010]$ , in good agreement with previous STM studies of the anatase  $\text{TiO}_2(101)$  surface.<sup>13,14,23,24</sup> A ball-and-stick model of the nonreconstructed (101)( $1 \times 1$ ) termination of the bulk is displayed in plan and side views in Figure 1c. Red atoms are oxygen, blue titanium. Flat terraces of anatase  $\text{TiO}_2(101)$  have a sawtooth corrugation as seen in the lower panel of Figure 1c, composed of 5- and 6-fold-coordinated Ti atoms ( $\text{Ti}_{5c}$ ,  $\text{Ti}_{6c}$ ) and 2- and 3-coordinated O atoms ( $\text{O}_{2c}$ ,  $\text{O}_{3c}$ ). The surface unit cell is also displayed in Figure 1c, with dimensions of  $10.24 \text{ \AA} \times 3.78 \text{ \AA}$ . It is important to note that a unique assignment of the direction of  $[10\bar{1}]$  cannot be determined from these LEED and STM results alone. To overcome this, Gong et al. conducted combined STM and first-principles calculations of the stability of various step structures on anatase (101).<sup>13</sup> In this study they found that the favored trapezoidal island and step directions reflect the underlying symmetry of the surface, thereby permitting assignment of the crystallographic directions. We have identified the same step structures in our STM images and have applied the results of ref 13 in our analysis, resulting in the assignment of the direction of  $[10\bar{1}]$  as shown in all of the figures.

Atomically resolved images were obtained on anatase  $\text{TiO}_2(101)$  using positive sample bias (empty states imaging) as displayed in Figure 2a. The origin of the contrast of this lattice has been identified by He et al.,<sup>14</sup> and it was shown that the bright features are actually derived from a  $\text{Ti}_{5c}$ – $\text{O}_{2c}$  pair. This is shown in the model in Figure 2b highlighted by yellow circles. The unit cell is marked on both the model and the STM image with a black rectangle, and the spacing as measured by STM is consistent with this explanation. An early observation of anatase  $\text{TiO}_2$  surfaces has been the low concentration of point defects at the surface, especially in comparison with rutile  $\text{TiO}_2$ .<sup>14</sup> Our images, e.g., that displayed in Figure 2a, reflect this, and only a few atomically sized imperfections are visible even after the samples are left in the residual vacuum for long periods of time.

**Low-Coverage Acetic Acid on Anatase  $\text{TiO}_2(101)$ .** The adsorption and bonding of carboxylic acids to  $\text{TiO}_2$  surfaces is of great interest, and extensive work has already been carried out on rutile  $\text{TiO}_2$  surfaces, the (110)( $1 \times 1$ ) termination in particular. The adsorption can be split into two main schemes, molecular and dissociative, depending on whether the carboxylic hydrogen

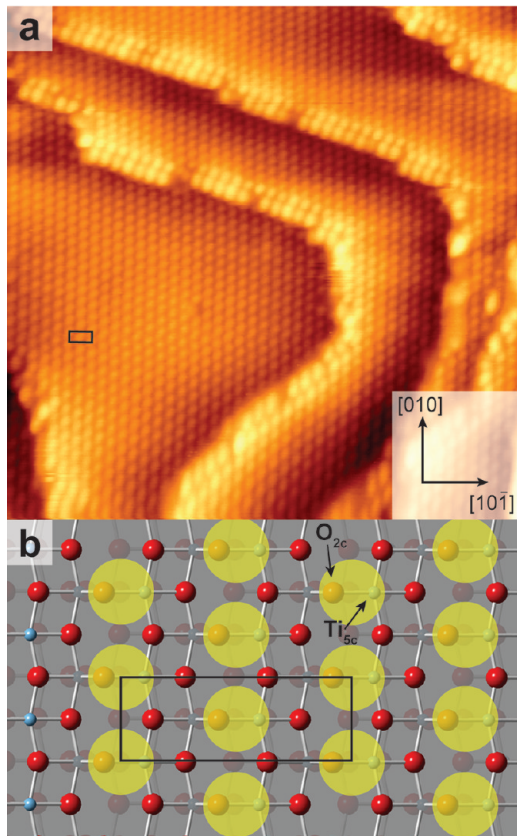


**Figure 2.** Atomically resolved empty states STM image of anatase  $\text{TiO}_2(101)$  and associated model showing the origin of the observed contrast. (a) Atomically resolved image ( $23 \times 23 \text{ nm}^2$ ,  $V_s = +1.2 \text{ V}$ ,  $I_t = 0.20 \text{ nA}$ ) where the bright atomically sized features correspond to  $\text{Ti}_{5c}-\text{O}_{2c}$  pairs. There is a very low density of defects or adsorbates observed. (b) Model of the anatase  $\text{TiO}_2(101)$  surface with the  $\text{Ti}_{5c}-\text{O}_{2c}$  pairs highlighted with yellow circles, which are the origin of the atomically sized features in (a). Key: red, oxygen; blue, titanium. The surface unit cell is marked with a black rectangle on the STM image and the model.

is lost. On rutile  $\text{TiO}_2(110)(1 \times 1)$ , acetic acid has been shown to adsorb dissociatively at room temperature with a number of possible bidentate binding geometries depending on the concentration of vacancies and other adsorbates on the surface. The most common geometry is found to be bidentate between adjacent  $\text{Ti}_{5c}$  sites along the rows in the  $[001]$  direction, leading to a  $(2 \times 1)$  acetate overlayer at saturation coverage.<sup>3,25</sup>

There is conflicting experimental and theoretical data regarding carboxylic acid adsorption on anatase surfaces, with both molecular and dissociative adsorption proposed. A key limitation for experimental studies has been the availability of good-quality anatase single crystals. Instead, anatase  $\text{TiO}_2$  films or nanoparticles have been more widely investigated, leading to results that are aggregates of many different faces and therefore require further deconvolution.<sup>26</sup> An example of such work is the study by Mattsson and Osterlund<sup>21</sup> of acetic acid adsorption on anatase nanoparticles using FTIR spectroscopy, where the signatures of both molecular and dissociative adsorption were observed. In refs 8 and 22 Tanner et al. used a combination of SPM and spectroscopic techniques to study formic and acetic acid on anatase  $\text{TiO}_2(001)(1 \times 4)$  and identified dissociated carboxylates forming a  $(2 \times 4)$  acetate superstructure. However, the binding geometry of individual molecules could not be satisfactorily explained with the data available. A number of

density functional theory (DFT) studies of formic acid adsorption on anatase  $(101)^{27-29}$  predict a different behavior, with a molecular monodentate geometry most favored. This is through the  $\text{C}=\text{O}$  oxygen to a  $\text{Ti}_{5c}$  site, with further stabilization provided by hydrogen bonding of the OH group to a neighboring  $\text{O}_{2c}$  atom.

Figure 3 shows a number of STM images of the anatase  $\text{TiO}_2(101)$  surface after exposure to 0.1 langmuir of acetic acid. The adsorbates appear as bright features  $\sim 170 \text{ pm}$  tall evenly distributed across the terraces and step edges as seen in Figure 3a, with the atomic lattice of the anatase faintly visible underneath. There is no apparent preference for adsorption on step edges, and the molecules are observed to exist as 2-D clusters and as isolated individuals, with a measured coverage of 0.06 ML indicating a high sticking probability. The mobility of the adsorbates is very low on the time scale of our experiments (hours), although some significant tip interactions are observed, characterized by streaking above the molecules in the fast scan direction (horizontal). The STM tip termination is well-known to have a large effect on the contrast observed in STM. This is evidenced in Figure 3b, where a spontaneous tip change occurs about halfway up the frame (marked with an arrow). In the lower half of the frame the acid molecules appear as seen in Figure 3a, bright round protrusions, but in the upper half a marked difference is observed.

Figure 3c is an atomically resolved STM image taken a couple of minutes later on the same area as that described above. In this imaging mode the adsorbates are characterized by an enhanced intensity (corresponding to a height of  $\sim 20-150 \text{ pm}$ ) of two neighboring  $\text{Ti}_{5c}-\text{O}_{2c}$  pairs in the  $[010]$  direction, with two further lobes of brightness pointing along the diagonals of the centered unit cell to the  $\text{Ti}_{5c}-\text{O}_{2c}$  pairs in the  $[11\bar{1}]$  and  $[1\bar{1}\bar{1}]$  directions with a dark spot between them. A drift-corrected image at higher resolution is shown in Figure 3d, with the bright spots of the lattice (unit cell marked with a black rectangle) originating from the  $\text{Ti}_{5c}-\text{O}_{2c}$  pairs as observed on the clean surface. Some of these pairs have been highlighted with yellow circles, showing clearly the plane of symmetry present within the molecules (marked with a dashed blue line). All of the adsorbate molecules are observed to have identical structures with the same orientation, suggesting only a single binding configuration. At the bottom center of Figure 3d, it is observed that two adsorbate molecules are bound on adjacent rows in the  $[10\bar{1}]$  direction, leading to the start of an ordered string pointing along  $[1\bar{1}\bar{1}]$ . To rule out the possibility that the STM contrast of the acetate was purely the result of a tip effect, the experiment was repeated using different tips, and for all tips a contrast similar to that of Figure 3d was observed. Dissociative adsorption of acetic acid results in hydrogen adatoms on the surface. However, their appearance in STM on anatase  $\text{TiO}_2(101)$  is not known, and we do not identify any features in our images that could be assigned to such species. The absence of such features in our STM images may be a result of their high mobility and reactivity under the experimental conditions (300 K). On the rutile  $\text{TiO}_2(110)$  surface, it has been shown that two hydroxyls resulting from dissociative acid absorption are able to abstract an oxygen atom from the surface, producing a water molecule which desorbs and leaving an oxygen vacancy behind.<sup>3</sup> Surface oxygen vacancies on anatase  $\text{TiO}_2(101)$  are rarely observed in STM due to their high reactivity and resultant short lifetimes,<sup>14</sup> so we might not expect to observe them during the course of our experiment, even if a similar dehydration reaction is occurring. Figure 4 shows three possible binding geometries for acetic acid on the anatase (101) surface:

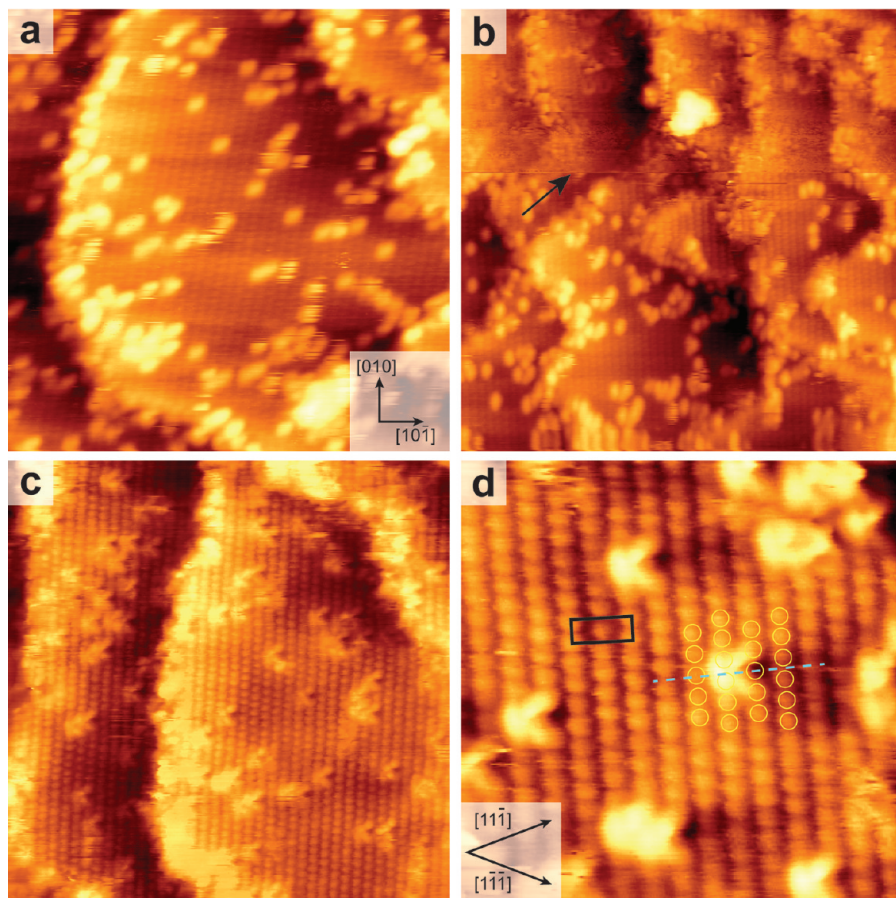


**Figure 3.** STM images of anatase  $\text{TiO}_2(101)$  at room temperature after exposure to 0.06 ML of acetic acid. (a) STM image ( $20 \times 20 \text{ nm}^2$ ,  $V_s = +1.5 \text{ V}$ ,  $I_t = 0.10 \text{ nA}$ ) of the normal imaging mode where individual adsorbates are imaged as bright features 170 pm tall, distributed evenly across the surface. (b) STM image ( $29 \times 29 \text{ nm}^2$ ,  $V_s = +1.5 \text{ V}$ ,  $I_t = 0.10 \text{ nA}$ ) showing a spontaneous tip change (marked with a black arrow) resulting in an imaging mode different from that of (a) with a new contrast of the acetate molecules. (c) Attributed resolved image ( $20 \times 20 \text{ nm}^2$ ,  $V_s = +0.8 \text{ V}$ ,  $I_t = 0.10 \text{ nA}$ ) of the acetate molecules in the high-contrast mode. The adsorbates are characterized by enhanced intensity above two neighboring  $\text{Ti}_{\text{sc}}-\text{O}_{2c}$  pairs along the  $[010]$  direction, with two further lobes of brightness pointing along the diagonals of the centered unit cell to the  $\text{Ti}_{\text{sc}}-\text{O}_{2c}$  pairs in the  $[11\bar{1}]$  and  $[1\bar{1}\bar{1}]$  directions and a dark spot between them. (d) Drift-corrected image ( $7 \times 7 \text{ nm}^2$ ,  $V_s = +1.0 \text{ V}$ ,  $I_t = 0.10 \text{ nA}$ ) of individual and paired acetate adsorbates. The surface unit cell is marked (black rectangle), and some  $\text{Ti}_{\text{sc}}-\text{O}_{2c}$  pairs are highlighted in yellow. The plane of symmetry of the acetate is marked with a dashed blue line.

(a) molecular monodentate binding through the  $\text{C}=\text{O}$  oxygen to a  $\text{Ti}_{\text{sc}}$  site, with the stabilizing hydrogen bond formed to the  $\text{O}_{2c}$  site in the same  $\text{Ti}_{\text{sc}}-\text{O}_{2c}$  pair, the intrapair arrangement, (b) molecular monodentate binding through the  $\text{C}=\text{O}$  oxygen to a  $\text{Ti}_{\text{sc}}$  site, with the stabilizing hydrogen bond formed to an  $\text{O}_{2c}$  site in a different  $\text{Ti}_{\text{sc}}-\text{O}_{2c}$  pair, the interpair arrangement, and (c) dissociative bidentate binding to two neighboring  $\text{Ti}_{\text{sc}}$  sites in the  $[010]$  direction, with the dissociated hydrogen bonded to a separate  $\text{O}_{2c}$  site. Since the position of the hydrogen adatom is unknown, has not been included in the model. Due to the symmetry observed in the STM appearance of individual molecules (see Figure 3d), the interpair molecular adsorption geometry (illustrated in Figure 4b) can be ruled out, leaving dissociative bidentate and intrapair molecular monodentate as the two most likely configurations at this stage. Theoretical modeling of formic acid on the anatase (101) surface presents a confusing picture as to the predicted stability of the various conformations. A number suggest that molecular monodentate (Figure 4b) is the most stable arrangement,<sup>27–29</sup> whereas others disagree and predict a bidentate arrangement (Figure 4c),<sup>30,31</sup> although it must be remembered that such calculations are only appropriate to 0 K, unlike our experiments, which are at room

temperature. One particular factor in the stability of the bidentate arrangement is the increased separation of the  $\text{Ti}_{\text{sc}}$  sites on anatase  $\text{TiO}_2(101)$  (3.78 Å) relative to rutile  $\text{TiO}_2(110)$  (2.96 Å), which could result in an increased strain of the binding.

**High-Coverage Acetic Acid on Anatase  $\text{TiO}_2(101)$ .** At higher coverages it is often observed that adsorbed molecules form ordered overlayers on  $\text{TiO}_2$  surfaces, such as that seen for azobenzene on anatase (101).<sup>32</sup> Figure 5 shows STM images of the results of exposing the anatase (101) surface to 2 langmuirs of acetic acid at (a) 300 K and (b) 420 K. The adsorbed molecules are imaged as bright spots (the same imaging mode as in Figure 3) covering the terraces of the substrate, with some small areas remaining uncovered in both cases. Analysis of the STM images yields nominal coverages of (a) 0.47 ML and (b) 0.40 ML. The small difference in coverage for these two cases despite the same exposure is accounted for by a slightly reduced sticking probability at the higher substrate temperature. In Figure 5a, as a result of exposure at room temperature, no long-range ordering of the adsorbates is observed. In Figure 5b, the result of adsorption at a raised substrate temperature has a general appearance similar to that seen in Figure 5a. However, there are a number of areas which display local ordering (highlighted in

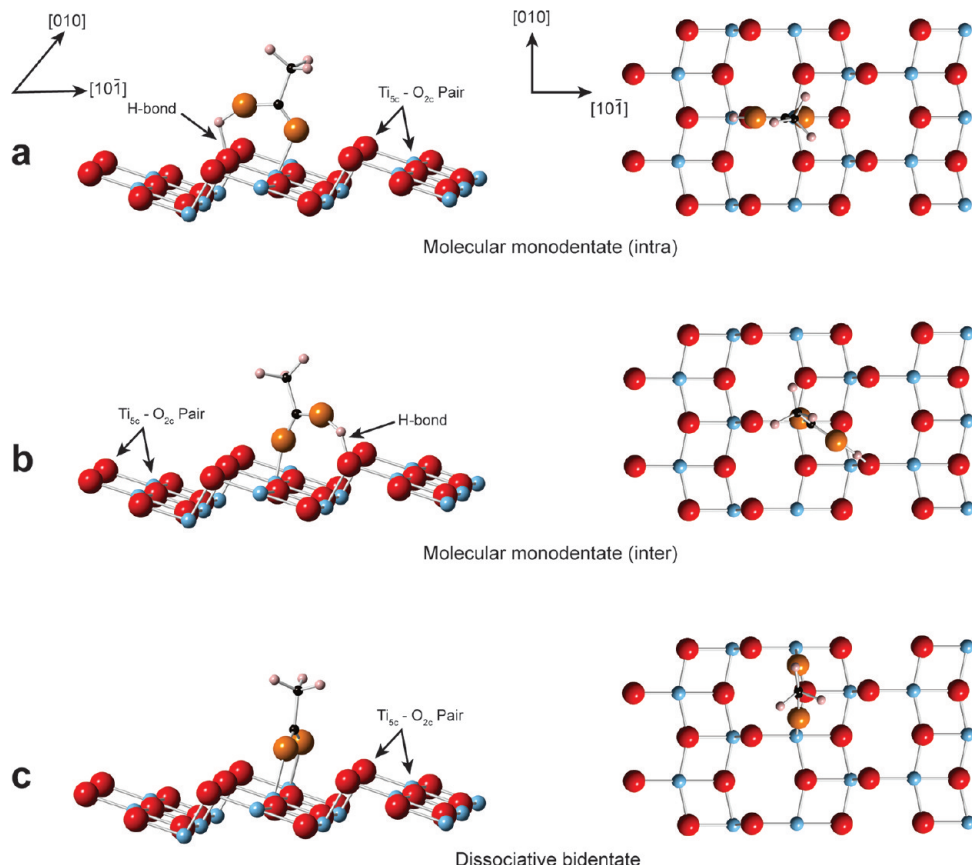


**Figure 4.** Ball-and-stick models showing possible binding configurations for acetic acid on anatase TiO<sub>2</sub>(101). (a) Molecular monodentate (intra) binding through the C=O oxygen to a Ti<sub>5c</sub> site, with the stabilizing hydrogen bond formed to the O<sub>2c</sub> site in the same Ti<sub>5c</sub>-O<sub>2c</sub> pair. (b) Molecular monodentate (inter) binding through the C=O oxygen to a Ti<sub>5c</sub> site, with the stabilizing hydrogen bond formed to an O<sub>2c</sub> site in a different Ti<sub>5c</sub>-O<sub>2c</sub> pair. (c) Dissociative bidentate binding to two neighboring Ti<sub>5c</sub> sites in the [010] direction, with the dissociated hydrogen bonded to a separate O<sub>2c</sub> site (the position of H is not indicated). Key: red, surface O; orange, acetate O; blue, Ti; black, C; pink, H. The models are based on those predicted in refs 27–29.

Figure 5b), both as short strings of molecules and as 2-D arrays forming two distinct domains. These ordered areas make up approximately 10% of the total surface area as measured by STM.

It is possible to image these areas of local ordering with higher resolution, images of which are presented in Figure 6a,c, and we are able to assign these areas as having a periodicity of (2 × 1). The red and blue line profiles across the superstructure in Figure 6a display intermolecular spacings of ~7.3 and ~5.7 Å, respectively, which correspond reasonably well with that expected for a (2 × 1) superstructure as displayed in the model in Figure 6b, where the blue circles represent the acetic acid molecules. The deviation in spacing is a result of a small amount of thermal or piezo drift in the STM image which could not be compensated for. Also illustrated in the model in Figure 6b are the two orientations possible with (2 × 1) periodicity along the diagonals of the centered unit cell (the [11̄1] and [1̄11] directions). An STM image showing a region of the sample containing adjacent overlayer domains is shown in Figure 6c. LEED investigations of this surface were carried out, but due to the small fraction of the overlayer that was ordered, no additional reflexes were observed. This rather low fraction of the surface covered by the (2 × 1) overlayer is perhaps an indication of a weak interaction along the [11̄1] and [1̄11] directions which results in small ordered domains. By comparison, on rutile TiO<sub>2</sub>(110) it has been proposed that the dissociated hydrogen bridges a pair of oxygen sites along [001] and is actually a factor

in inducing the observed long-range (2 × 1) periodicity across the rows (i.e., along the [1̄10] direction) for carboxylates.<sup>33</sup> In Figure 7, models are presented of two possible binding confirmations, dissociative bidentate (a) and molecular monodentate (intra) (b), where a hydrogen bond is formed between the acidic proton and the oxygen anion that is in the same Ti<sub>5c</sub>-O<sub>2c</sub> pair which bonds to the carboxyl oxygen in the acid. The dissociative bidentate geometry leads to a (2 × 1) overlayer at saturation, whereas the molecular monodentate (intra) geometry is able to form a (1 × 1) superstructure at saturation. Due to the appearance and spacing of the adsorbates in the STM image displayed in Figure 6c, where two domains are visible that are mirror images of each other (line of symmetry along [10̄1]), the assignment of a (2 × 1) superstructure is clear. Our STM observations at both high and low coverages lead us therefore to conclude that the most likely binding geometry is that of dissociative bidentate between two Ti<sub>5c</sub> sites in the [010] direction. The low observed mobility of the acetate during the course of our experiments at 300 K is comparable with that for the bidentate binding of carboxylates on rutile TiO<sub>2</sub>(110)<sup>34</sup> and is also suggestive of a relatively strong interaction with the anatase TiO<sub>2</sub>(101) surface. An additional consideration is the potential for coverage-dependent changes in binding depending on the functionality of the adsorbate molecule as has been observed for terephthalic acid on rutile TiO<sub>2</sub>(110).<sup>35</sup> The addition of two extra functional moieties (a benzene ring and an

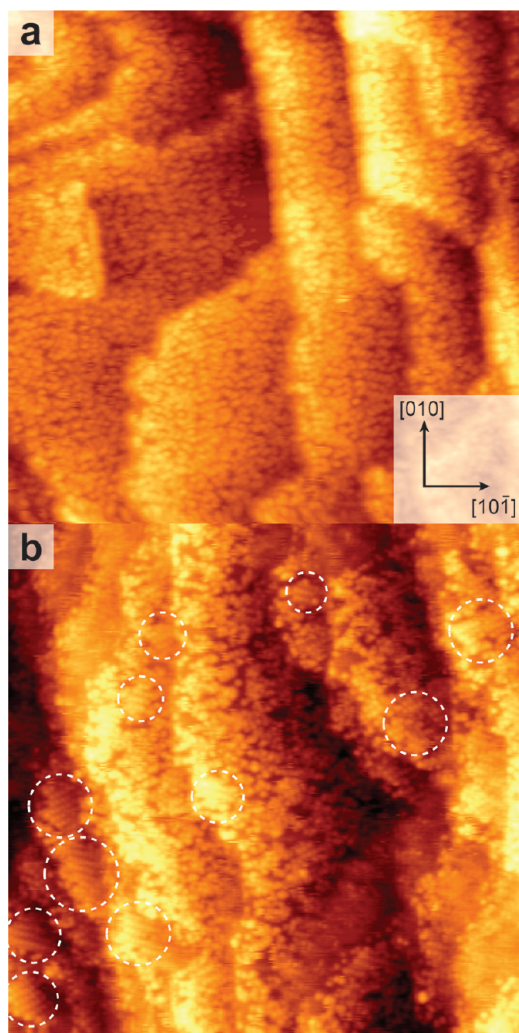


**Figure 5.** STM images of 2 langmuirs of acetic acid exposure on anatase  $\text{TiO}_2(101)$  at (a) 300 K and (b) 420 K. (a) The acetic acid forms a 0.47 ML overlayer with no apparent long-range ordering ( $39 \times 39 \text{ nm}^2$ ,  $V_s = +1.2 \text{ V}$ ,  $I_t = 0.40 \text{ nA}$ ). (b) At higher substrate temperatures a 0.4 ML overlayer is formed with ordered domains covering ~10% of the surface area with two orientations (marked with white dashed circles) ( $50 \times 50 \text{ nm}^2$ ,  $V_s = +1.4 \text{ V}$ ,  $I_t = 0.10 \text{ nA}$ ).

additional carboxylate group) compared to acetic acid leads to the ability to form significant intermolecular interactions which stabilize monodentate binding at low coverage and bidentate binding at saturation. There is no reported evidence in the literature to suggest that acetic acid on rutile  $\text{TiO}_2(110)$  displays any significant binding changes on moving to higher coverage, and as a result, any intermolecular interactions are assumed to be rather minor and unlikely to effect a change in binding on the anatase  $\text{TiO}_2(101)$  surface.

**Surface Modification of Acetic Acid on Anatase  $\text{TiO}_2(101)$ .** STM has a unique ability to modify surfaces with extreme precision, one of the simplest ways being to apply a voltage pulse to the tip at a certain point during scanning. Such voltage pulsing has been used to good effect on rutile  $\text{TiO}_2(110)$  to selectively desorb H atoms by applying a +3 V pulse for 300 ms and even induce reconstructions at higher bias voltages and currents.<sup>36</sup> We have used voltage pulsing to attempt to selectively desorb acetic acid from the anatase (101) surface, the results of which are displayed in Figure 8a. The anatase  $\text{TiO}_2(101)$  surface was exposed to 2 langmuirs of acetic acid at room temperature,

yielding a 0.47 ML coverage similar to that displayed in Figure 5a, with no apparent ordering of the adsorbates. Figure 8a is a  $22 \times 22 \text{ nm}^2$  STM image obtained after a +6 V pulse was applied for 1 s at the position marked with “x”. It is observed that an area of diameter ~6 nm (marked with a dashed circle) has been mostly cleared of adsorbates, with the atomic lattice now visible underneath (unit cell marked in blue). A number of adsorbates with larger dimensions than single acetate molecules are observed inside the cleared region and around its perimeter. These are assigned to clusters of acetate molecules formed as a result of the pulse, although their precise identity is not known. No additional ordering of the acetate is observed in the surrounding area of the pulse, although the tip apex is likely to have been affected and there is a slight additional convolution effect present, which may hinder the image quality. Voltage pulses lower than +6 V did not affect the overlayer, although further investigations are required to analyze the effect of the pulse duration and current. It is of interest to note that there does not appear to have been any effects of the pulse on the underlying structure of the anatase  $\text{TiO}_2(101)$ . This is in contrast with results on rutile  $\text{TiO}_2(110)(1 \times 1)$  where voltage pulses above +5 V lead to a  $(1 \times 2)$  reconstruction of the surface in the immediate area around the position of the pulse.<sup>36</sup>

As observed previously in this study, the temperature of the substrate during deposition can have a significant effect on the structure of the adsorbed species. To investigate the desorption behavior of acetic acid on anatase  $\text{TiO}_2(101)$ , a sample with a coverage of 0.4 ML of acetic acid was heated to 570 K in UHV for 10 min. An STM image obtained after this heating is displayed in Figure 8b. Most of the acetic acid is observed to have been desorbed cleanly, with the residual coverage measured at 0.05 ML, of which 80% is located at the step edges. Such preferential desorption at the terrace sites over those molecules bound at step edges suggests enhanced bonding of the acetate at such locations, possibly due to undercoordinated Ti atoms. The molecularly sized features remaining after the desorption are observed to have the same height and width as a single acetate molecule, and it can therefore be assumed that if any dissociation took place during heating, all products were desorbed. The UHV system used for this study was not equipped to perform temperature-programmed desorption (TPD) investigations, and as a result, it is not known whether the acetate was desorbed molecularly or if it dissociated upon heating. TPD and STM measurements by Tanner et al. of formic and acetic acid on anatase  $\text{TiO}_2(001)(1 \times 4)$  showed desorption of the acetic acid upon annealing to 850 K, again with only a low concentration of adsorbates and dissociation products remaining on the surface.<sup>8,22</sup> The mechanism behind desorption by heating or pulsing is unknown for acetate on anatase  $\text{TiO}_2(101)$ , but it may proceed via one of the routes detailed in the review by Pang et al. which result in a number of reaction products rather than desorption of acetate as an intact molecule.<sup>3</sup> Thermal desorption experiments of acetate from rutile  $\text{TiO}_2(110)$  and  $\text{TiO}_2(001)(2 \times 1)$  surfaces have suggested that ketene is the major reaction product with evidence that some oxygen remains and reacts with the surface.<sup>25</sup>

## CONCLUSIONS

In summary, we present scanning tunneling microscopy investigations of the adsorption properties of acetic acid on anatase  $\text{TiO}_2(101)$ . A clean anatase (101) substrate was characterized with atomic resolution STM, LEED, and AES. At small exposures at room temperature, acetic acid was found to adsorb evenly across the substrate terraces with no apparent

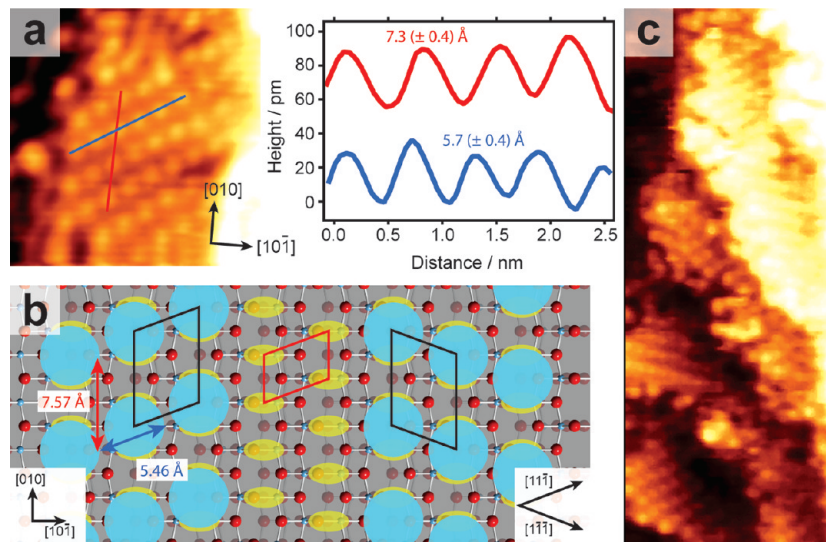


**Figure 6.** STM images and structural models explaining the origin of the ordered acetic acid domains on anatase  $\text{TiO}_2(101)$ . (a) STM image ( $7 \times 7 \text{ nm}^2$ ,  $V_s = +1.4 \text{ V}$ ,  $I_t = 0.10 \text{ nA}$ ) of one such region of ordering. The associated line profiles confirm a  $(2 \times 1)$  superstructure. (b) Structural model of the anatase  $\text{TiO}_2(101)$  surface with a  $(2 \times 1)$  overlayer. The blue circles represent individual acetate adsorbates and the yellow ovals the  $\text{Ti}_{\text{sc}}-\text{O}_{2c}$  pairs that are the origin of the atomic contrast on clean anatase  $\text{TiO}_2(101)$  such as observed in Figures 2 and 3. The primitive unit cell of the surface is shown in red, and the unit cells of the  $(2 \times 1)$  acetate domains are in black. The acetate superstructure can be oriented in two directions along the diagonals of the centered unit cell ( $[1\bar{1}\bar{1}]$  and  $[\bar{1}\bar{1}\bar{1}]$ ), forming two possible domains as indicated. (c) STM image ( $10 \times 25 \text{ nm}^2$ ,  $V_s = +1.2 \text{ V}$ ,  $I_t = 0.40 \text{ nA}$ ) showing clearly the two domains of the ordered acetate.

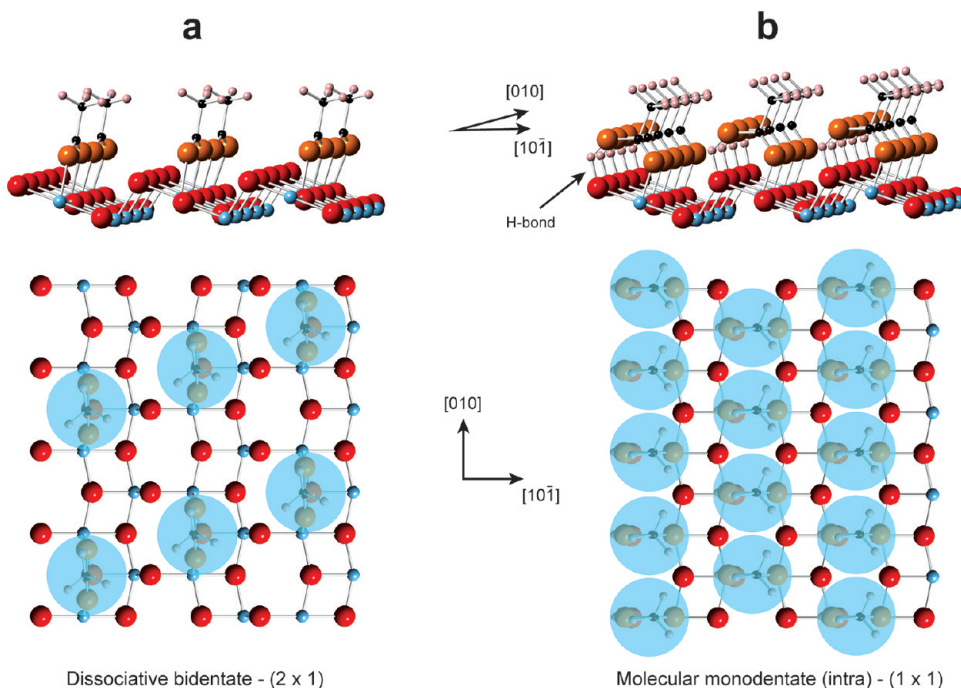


**Figure 7.** Ball-and-stick models of acetate on the anatase  $\text{TiO}_2(101)$  at a saturated coverage in (a) dissociated bidentate and (b) molecular monodentate (intra) geometries. The dissociated bidentate geometry yields a  $(2 \times 1)$  superstructure at a total adsorbate coverage of 0.5 ML, which is most consistent with the STM results displayed in Figures 5 and 6. The molecular monodentate (intra) arrangement, where the acid forms a hydrogen bond to the substrate, would be expected to form a  $(1 \times 1)$  overlayer with a 1 ML coverage at saturation. Key: red, surface O; orange, acetate O; blue, Ti; black, C; pink, H.

preference for step edges. At saturation coverages after deposition at room temperature there was no long-range ordering of the adsorbates, although exposure at raised substrate temperatures induced regions of highly ordered superstructure in STM. The periodicity of such overlayers was determined to be  $(2 \times 1)$ , and along with high-resolution STM imaging of individually adsorbed molecules, the adsorption was consistent

with a dissociated bidentate binding geometry of the acetate to two neighboring  $\text{Ti}_{\text{sc}}$  atoms along the  $[010]$  direction. The acetate molecules were observed to have low mobility at the temperature of our investigations (300 K), although there were considerable interactions with the tip under the tunneling conditions employed. Voltage pulsing of +6 V with the STM tip was able to desorb acetate molecules from the surface, as was

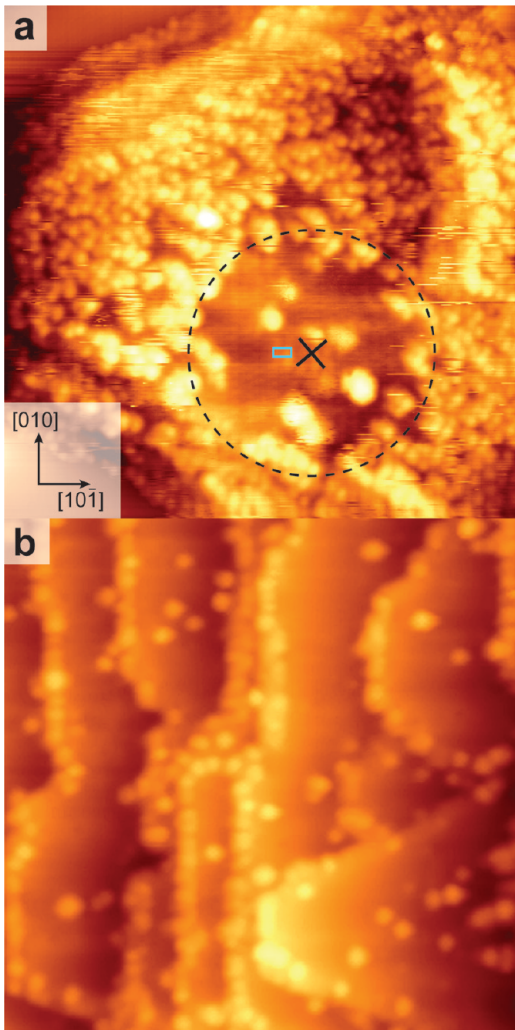


**Figure 8.** STM images of surface modification of acetate on anatase  $\text{TiO}_2(101)$  by (a) tip pulsing and (b) heating in UHV. In both cases, a 0.4 ML overlayer of acetate was formed which was similar in appearance to that shown in Figure 5a. (a) STM image ( $22 \times 22 \text{ nm}^2$ ,  $V_s = +1.2 \text{ V}$ ,  $I_t = 0.10 \text{ nA}$ ) after a +6 V tip pulse applied at the position marked with “X”. A circular area (dashed line) of diameter  $\sim 6 \text{ nm}$  has been cleared of most adsorbates with the atomic lattice visible in the clear area (surface unit cell marked in blue). (b) STM image ( $30 \times 30 \text{ nm}^2$ ,  $V_s = +1.4 \text{ V}$ ,  $I_t = 0.10 \text{ nA}$ ) recorded after the acetate-covered surface was heated to 570 K in UHV for 10 min. The coverage of remaining acetate is estimated to be 0.05 ML, and it is predominantly located at the step edges of the substrate.

heating to  $\sim 570 \text{ K}$  in UHV. Desorption by heating at this temperature removed the majority of the adsorbates; the remainder were observed to be located primarily at the step edges of the anatase substrate, suggesting enhanced bonding at these sites.

## AUTHOR INFORMATION

### Corresponding Author

\*Phone: +44 (0)20 7679 7979. Fax: +44 (0)20 7679 0595. E-mail: g.thornton@ucl.ac.uk.

### Notes

The authors declare no competing financial interest.

## ACKNOWLEDGMENTS

We thank Patrick Nickels and Chi Lun Pang for useful discussions. This work was funded by the European Union - Initial Training Network grant SMALL and a European Research Council Advanced grant (G.T.).

## REFERENCES

- (1) Fujishima, A.; Zhang, X.; Tryk, D. *Surf. Sci. Rep.* **2008**, *63*, 515–582.
- (2) Diebold, U. *Surf. Sci. Rep.* **2003**, *48*, 53–229.
- (3) Pang, C. L.; Lindsay, R.; Thornton, G. *Chem. Soc. Rev.* **2008**, *37*, 2328–2353.
- (4) Henderson, M. A. *Surf. Sci. Rep.* **2011**, *66*, 185–297.
- (5) Thompson, T. L.; Yates, J. T. *Chem. Rev.* **2006**, *106*, 44284453.
- (6) Yates, J. T. *Surf. Sci.* **2009**, *603*, 1605–1612.
- (7) Fujishima, A.; Honda, K. *Nature* **1972**, *238*, 37–38.
- (8) Tanner, R.; Liang, Y.; Altman, E. *Surf. Sci.* **2002**, *506*, 251–271.
- (9) Herman, G.; Gao, Y. *Thin Solid Films* **2001**, *397*, 157–161.
- (10) He, Y.; Tilocca, A.; Dulub, O.; Selloni, A.; Diebold, U. *Nat. Mater.* **2009**, *8*, 585–589.
- (11) Herman, G.; Dohnalek, Z.; Ruzycki, N.; Diebold, U. *J. Phys. Chem. B* **2003**, *107*, 2788–2795.
- (12) Gong, X.-Q.; Selloni, A.; Dulub, O.; Jacobson, P.; Diebold, U. *J. Am. Chem. Soc.* **2008**, *130*, 370–381.
- (13) Gong, X.-Q.; Selloni, A.; Batzill, M.; Diebold, U. *Nat. Mater.* **2006**, *5*, 665–670.
- (14) He, Y.; Dulub, O.; Cheng, H.; Selloni, A.; Diebold, U. *Phys. Rev. Lett.* **2009**, *102*, 106105.
- (15) O'Regan, B.; Graetzel, M. *Nature* **1991**, *353*, 737–740.
- (16) Hara, K.; Horiuchi, H.; Katoh, R.; Singh, L.; Sugihara, H.; Sayama, K.; Murata, S.; Tachiya, M.; Arakawa, H. *J. Phys. Chem. B* **2002**, *106*, 374–379.
- (17) Ikeda, S.; Sugiyama, N.; Pal, B.; Marci, G.; Palmisano, L.; Noguchi, H.; Uosaki, K.; Ohtani, B. *Phys. Chem. Chem. Phys.* **2001**, *3*, 267–273.
- (18) Kim, Y.; Walker, J.; Samuelson, L.; Kumar, J. *Nano Lett.* **2003**, *3*, 523–525.
- (19) Nazeeruddin, M.; Kay, A.; Rodicio, I.; Humphrybaker, R.; Muller, E.; Liska, P.; Vlachopoulos, N.; Gratzel, M. *J. Am. Chem. Soc.* **1993**, *115*, 6382–6390.
- (20) Villarreal, T.; Gomez, R.; Neumann-Spallart, M.; Alonso-Vante, N.; Salvador, P. *J. Phys. Chem. B* **2004**, *108*, 15172–15181.
- (21) Mattsson, A.; Osterlund, L. *J. Phys. Chem. C* **2010**, *114*, 14121–14132.
- (22) Tanner, R.; Sasahara, A.; Liang, Y.; Altman, E.; Onishi, H. *J. Phys. Chem. B* **2002**, *106*, 8211–8222.
- (23) Dulub, O.; Diebold, U. *J. Phys.: Condens. Matter* **2010**, *22*, 084014.
- (24) Hebenstreit, W.; Ruzycki, N.; Herman, G.; Gao, Y.; Diebold, U. *Phys. Rev. B* **2000**, *62*, 334–336.
- (25) Tao, J.; Luttrell, T.; Bylsma, J.; Batzill, M. *J. Phys. Chem. C* **2011**, *115*, 3434–3442.
- (26) Wang, C.; Groenzin, H.; Shultz, M. *J. Am. Chem. Soc.* **2005**, *127*, 9736–9744.
- (27) Miller, K. L.; Musgrave, C. B.; Falconer, J. L.; Medlin, J. W. *J. Phys. Chem. C* **2011**, *115*, 2738–2749.
- (28) Miller, K. L.; Falconer, J. L.; Medlin, J. W. *J. Catal.* **2011**, *278*, 321–328.
- (29) Vittadini, A.; Selloni, A.; Rotzinger, F.; Gratzel, M. *J. Phys. Chem. B* **2000**, *104*, 1300–1306.
- (30) Luschnitz, R.; Gemming, S.; Seifert, G. *Eur. Phys. J. Plus* **2011**, *126*, 98–111.
- (31) Raghunath, P.; Lin, M. C. *J. Phys. Chem. B* **2008**, *112*, 8276–8287.
- (32) Li, S.-C.; Diebold, U. *J. Am. Chem. Soc.* **2010**, *132*, 64–66.
- (33) Lyubinetsky, I.; Yu, Z. Q.; Henderson, M. A. *J. Phys. Chem. C* **2007**, *111*, 4342–4346.
- (34) Onishi, H. *Springer Ser. Chem. Phys.* **2003**, *70*, 75–90.
- (35) Rahe, P.; Nimmrich, M.; Nefedov, A.; Naboka, M.; Woll, Ch.; Kuhnle, A. *J. Phys. Chem. C* **2009**, *113*, 17471–17478.

(36) Pang, C. L.; Bikondoa, O.; Humphrey, D. S.; Papageorgiou, A.; Cabailh, G.; Ithnin, R.; Chen, Q.; Muryn, C. A.; Onishi, H.; Thornton, G. *Nanotechnology* **2006**, *17*, 5397–5405.